文章编号：1001-9014(XXXX)XX-0001-17

DOI：10. 11972/j. issn. 1001-9014. JIMW. 2026190

Photonics-assisted Millimeter-wave and Terahertz communications for 6G: Advances, challenges, and prospects

Jia Jun-Lian， Dong Bo-Yu， Chi Nan， Zhang Jun-Wen*

（Key Laboratory for Information Science of Electromagnetic Waves（MoE），College of Future Information Technology，Fudan University，Shanghai 200433，China）

Abstract：This review examines recent advances in photonics-assisted millimeter-wave and terahertz communications for 6G and analyzes the associated device- and system-level challenges. Representative architectures and experimental results are compared in terms of optoelectronic conversion，carrier generation，key devices，waveform processing，multidimensional multiplexing，beamforming，and integrated sensing and communication. Photonic approaches provide broadband and frequency-agile carrier generation，low-loss fiber distribution，coherent-reference sharing，and true-time-delay beamforming，while current limitations include output power，conversion efficiency，packaging，real-time digital signal processing，energy consumption，and manufacturability. Hybrid optoelectronic integration can support high-capacity fiber-wireless systems，but the architecture must be chosen according to the link budget，total system power，and integration requirements of the application.

Key words：6G，photonics-assisted communication，millimeter-wave communication，terahertz communication，fiber-wireless integration

PACS:

Introduction

Sixth-generation wireless communication（6G）is an advanced communication system intended for deployment in the 2030s[1]. Looking forward to connecting everything with ultra-high speed，ultra-reliable connections，and intelligent technologies，6G will lay a solid foundation for an era in which communication and intelligence are ubiquitous. In fifth-generation（5G），three major categories of usage scenarios are defined. Continuous evolutions of these three scenarios will be integrated into 6G，and 6G is predicted to go beyond them[1]. As illustrated in Figure 1，enhanced mobile broadband（eMBB+）will introduce extended reality（xR）applications for entertainment，manufacturing，and medical treatment，requiring massive link resources. Massive machine-type communication（mMTC+）will be widely deployed in smart cities，traffic，industry，and so on，urging the fusion of sensing in communication systems. Ultra-reliable low-latency communications（URLLC+）will impose more stringent latency and reliability requirements，supporting new applications such as unmanned aerial vehicles and robots.

As communication requirements continue to increase，6G will require new radio access technologies（RATs）with sufficient spectrum resources and system capabilities[2-4]. Millimeter-wave（mmWave）and tera-

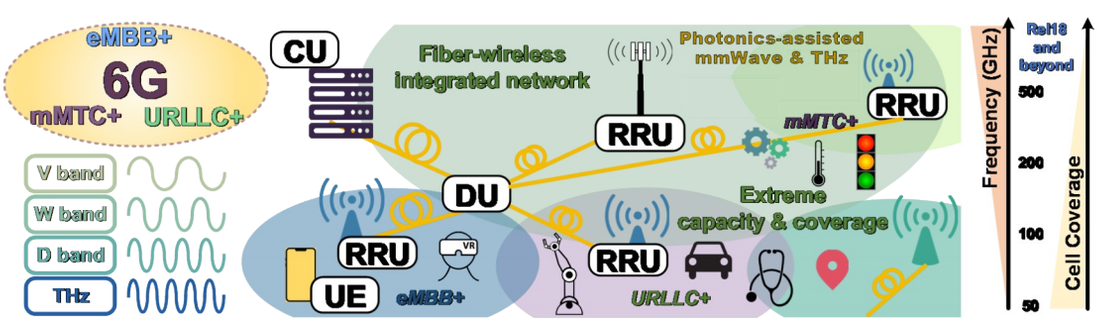

Fig. 1 6G radio access networks（RAN）with fiber-wireless integrated mmWave and THz communications
图 1 光纤—无线融合毫米波与太赫兹通信的6G无线接入网（RAN）

Received date：2026-XX-XX，　　收稿日期：2026-录用日期：2026-

Foundation items：Supported by the National Natural Science Foundation of China（62235005，62525102）；China Postdoctoral Science Foundation under Grant（2025M783505）.

* **Corresponding author**：E-mail：junwenzhang@fudan. edu. cn

hertz (THz) communication systems use wireless carriers from 30 GHz to beyond 1 THz and are among the candidate technologies for 6G, attracting great attention from the global industry and academic research institutions. As a potential RAT for 6G, the International Telecommunication Union (ITU) has identified high-frequency spectrum and extreme-capacity links as relevant elements of the IMT-2030 framework[5].

For discussion in this review, the spectrum is grouped into four engineering ranges, each with a distinct balance between available bandwidth and implementation maturity[3-5]. The 30-100 GHz range benefits from comparatively mature radio-frequency (RF) front ends and antennas, while photonics contributes most directly to low-loss distribution and true-time-delay beamforming. Between 100 and 300 GHz, large contiguous bandwidths support 100-Gbit/s-class links, but amplifier performance, propagation loss, and packaging parasitics become increasingly restrictive. This range is therefore particularly relevant to D- and F-band backhaul, data-room links, and short-range extreme-capacity access.

At 0.3-1 THz, optical heterodyning provides frequency agility and very wide signal bandwidth, making the range attractive for short line-of-sight links, interconnects, and high-resolution sensing. The corresponding link budget is constrained by source power, receiver sensitivity, molecular absorption, antenna alignment, and package loss. Above 1 THz, the spectral and sensing potential remains substantial, but practical communication systems are limited by the maturity of sources, detectors, modulators, waveguides, and packaging. These layers are used here as an engineering framework rather than as replacements for formal ITU or IEEE definitions.

In the physical layer, fiber-wireless integration is a key technology that supports radio access networks (RAN) in 6G. The links among the central unit (CU), distributed units (DUs), and remote radio units (RRUs) are based on an optical fiber network of low complexity and high capacity. Photonics-assisted mmWave and THz technologies make it possible to generate wireless signals directly from optical signals, eliminating high-frequency electronic oscillators and mixers at the remote site. Photonic generation and modulation can provide broad bandwidth and frequency agility, depending on the modulator and photomixer platform. Optical fiber also provides substantially lower distribution loss than electrical cables at very high carrier frequencies. Photonics-assisted architectures can therefore improve remote signal distribution and reduce the amount of high-frequency electronic hardware required at the RRU[6-7].

Light sources, photonic mixers, and modulators form the principal optoelectronic interfaces of mmWave and THz communication systems. Their phase noise, bandwidth, saturation power, conversion efficiency, and packaging directly constrain system performance and deployment. Considering the seamless integration of mmWave and THz wireless communication and the optical fiber network, especially in the mobile backhaul network application of 6G communication, photonic transceiver integration offers high flexibility, compact implementation, low latency, and low complexity, while facilitating the convergence of optical-fiber and wireless communication.

Integrated dual-laser sources, optical frequency-division schemes, modified uni-travelling-carrier (MUTC) photodiodes, thin-film lithium-niobate interfaces, and plasmonic or graphene devices improve compactness, carrier coherence, optoelectronic interfacing, and bidirectional conversion in fiber-wireless architectures[8-18].

In this article, we review the advances, challenges, and prospects in mmWave and THz communications, specifically focusing on photonics-assisted systems. Section 1 reviews system architectures, representative transmission experiments, photonic O/E – E/O conversion, optoelectronic devices, waveform and signal processing, and multidimensional multiplexing as advances in photonics-assisted mmWave and THz communications. Section 2 discusses the propagation, conversion, device, coherence, processing, beam-control, and integration challenges that are specific to or coupled with photonic systems. Section 3 outlines prospects in photonic antenna arrays, beamforming, native artificial intelligence, and integrated sensing and communication. Section 4 concludes the review.

1 Advances in photonics-assisted mmWave and THz communications for 6G

Section 1 examines how the location of frequency conversion and processing affects link performance. The transmission results are followed by a discussion of conversion mechanisms, devices, waveforms, and multiplexing, with attention to the constraint each approach addresses and the limits that remain.

1.1 System architectures

In the last two decades, many studies have been carried out to achieve ultra-high-speed wireless communications based on mmWave and THz frequencies, targeting extremely high-speed communication beyond 100 Gbit/s. Among all these studies and demonstrations, there are two main categories of approaches: the traditional electronic-based solution and the photonics-assisted solution. The former uses solid-state electronic devices, e.g., transceivers implemented in CMOS or other monolithic microwave integrated-circuit (MMIC) technologies. As shown in Figure 2, the traditional electronic-based mmWave and THz transceivers generally consist of a local oscillator (LO) realized by a multiplier chain from a lower frequency source to the mmWave or THz bands, and an electrical mixer for baseband signal modulation. Alternatively, photonics-assisted mmWave and THz communication systems can be implemented using photonic up- and down-conversion. Photonic up-conversion can be implemented through optical heterodyning to perform the optical-to-mmWave/THz process, while the photonic down-conversion can be realized by the coherent detection of the optically modulated mmWave/THz signals, with a LO frequency-shifted to the modulated op-

tical sideband. Photonic components provide wide bandwidths for modulation and mixing, but the output power is limited compared to their electronic counterparts.

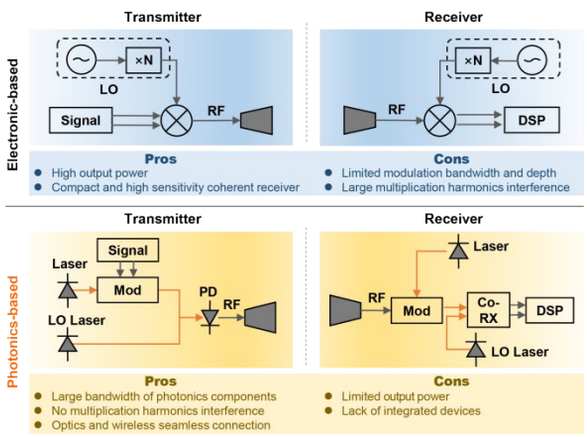

Fig. 2 Architectures of electronic and photonics-assisted solutions of transmitter and receiver in mmWave and THz communication systems (LO: local oscillator, RF: radio frequency, DSP: digital signal processing, Mod: modulator, Co-Rx: coherent receiver)
图 2 毫米波与太赫兹通信系统中基于电子和光子技术的发射机与接收机架构(LO:本地振荡器;RF:射频;DSP:数字信号处理;Mod:调制器;Co-Rx:相干接收机)

To support the dense deployment of RRUs, photonics-assisted systems are proposed as they are naturally suitable for fiber-wireless integration because of their optical-to-electrical and electrical-to-optical (OE/EO) conversion processes, as shown in Figure 3. There are five main components in a photonics-assisted complex signal mmWave or THz system: the light sources, baseband signal modulator, photonic mixer, receiving modulator, and coherent receiver. The laser sources determine the center frequency as well as the quality of the transmitting signal, the baseband signal modulator determines the bandwidth of the transmitting signal, and the photonics mixer, which is usually UTC-PD or positive-intrinsic-negative (PIN)-PD, and the receiving modulators are the key components enabling higher frequency of the signal.

All baseband processing functions, including multi-wavelength generation, baseband modulation, coherent reception, and multiplexing, are concentrated at the CU. The RRUs therefore primarily perform O/E and E/O conversion, together with the required analog front end, antenna, bias, and control functions. All the RRUs are photonics-assisted transceivers, consisting of the photonic mixer, receiving modulator, and analog front ends. Currently, electronic-based transceivers are mainly used in UEs because of the current lack of integrated photonic components. Electronic-based transceivers, instead, have the advantage of compact integration[19]. The overall architecture mixes photonic and electronic components, and supports coordinated optical-fiber distribution and mmWave/THz wireless access. The use of a fiber optic distribution network enables the ultra-dense deployment of mmWave and THz over large covered areas and ensures ultra-high-speed and high-capacity for 6G[2,20-24]. The preferred architecture depends on whether the dominant constraint is RF power and sensitivity, optical distribution, or broadband conversion.

1.2 High-capacity transmission demonstrations

Both architectures have been demonstrated for extremely high-speed wireless access. Figure 4[3,19,25-27] compares representative electronic, hybrid electronic-photonic, and all-photonic demonstrations in terms of carrier frequency and per-antenna data rate. Here, "all-photonic" denotes photonic conversion at both wireless interfaces; electronic amplification, data conversion, control, and DSP may still be required. It highlights the overall relationship among system architecture, operating frequency, and transmission capacity. A 105-Gbit/s transmitter operating in the 300-GHz band was implemented in a 40-nm CMOS process[28]. For mmWave and THz communications, photonics-assisted demonstrations have achieved some of the highest reported rates, particularly where broad optical bandwidth and frequency agility are exploited in terms of transmission speed owing to the large bandwidth, high modulation order, lower harmonic interference, and tunability, as shown in Figure 4. Photonic-transmitter/electronic-receiver demonstrations include 200 Gbit/s at 92.5 GHz[25] and approximately 300 Gbit/s gross rate per polarization across the 320 – 380-GHz band, yielding 612.65 Gbit/s aggregate gross rate and 510.5 Gbit/s net rate with two polarizations[29]. With multidimensional multiplexing and advanced digital sig-

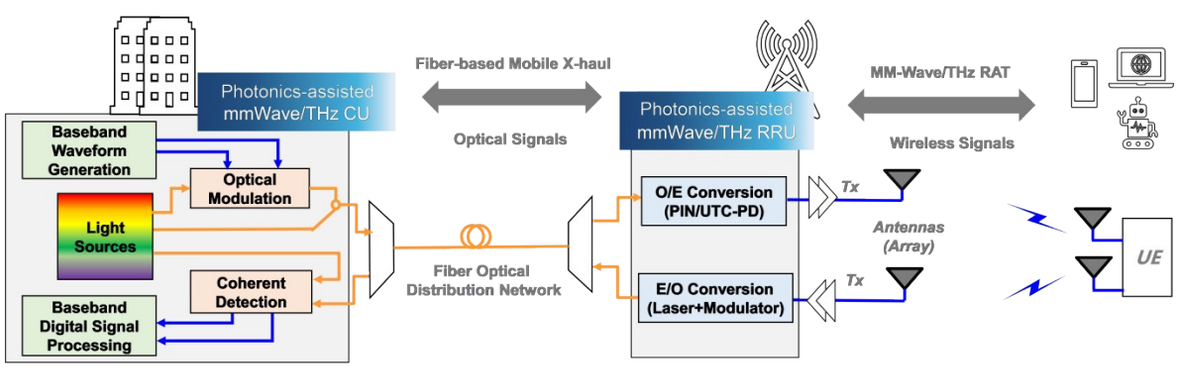

Fig. 3 Architecture of the fiber-wireless-integrated network in photonics-assisted mmWave and THz 6G system
图 3 光子辅助毫米波与太赫兹 6G 系统中的光纤—无线融合网络架构

nal processing (DSP), aggregate capacities of above 0.2 Tbit/s have been demonstrated[19,25-27]. With the development of a high-speed electro-optical modulator, transparent optical fiber to mmWave and THz, and mmWave and THz to optical fiber links have also been demonstrated[26-27]. As shown in Figure 4, the all-photonic transmitter-and-receiver solutions have achieved 71.4 Gbit/s at 0.1 THz[26] and 240 Gbit/s at 0.231 THz[27], respectively. These demonstrations have paved the road for bidirectional conversion between optical fiber and mmWave/THz wireless links, making seamless fiber-wireless integration possible in 6G RAN.

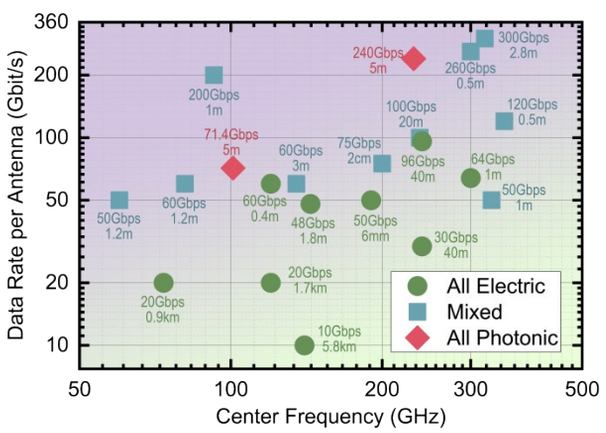

Fig. 4 Data-rate comparison of representative electronic, hybrid electronic-photonic, and all-photonic mmWave and THz communication systems
图4 代表性的电子、光电混合以及全光子毫米波、太赫兹通信系统的速率对比

Communication at 560 GHz has been demonstrated at 112 Gbit/s over 10 mm[30]. Device-level THz-to-optical detection over 0.5 – 2.5 THz[31] demonstrates a wider conversion range, but does not establish a data-link rate at every frequency. A separate quantum cascade laser (QCL)-based experiment at a dominant emission frequency of 2.4 THz transmitted 4-Gbit/s NRZ-OOK over 0.5 m[32]. It used a 19-K source and a room-temperature Schottky detector; about 40 μW received power reached the reported pre-FEC threshold of 3.8×10^{-3}. This cryogenic laser link is listed separately from telecom-band optical-heterodyne systems.

Representative systems span integrated transceivers, complete fiber-wireless-fiber links, high-capacity spatial multiplexing, and long-reach wireless transmission. An integrated dual-DFB photonic chip generated a high-purity 408-GHz carrier and supported 131.21 Gbit/s net-rate transmission over 10.7 m[8]. A graphene-integrated optoelectronic mixer demonstrated compact 93-GHz wireless conversion[9], while a thin-film-lithium-niobate platform provided reconfigurable operation from 0.5 to 115 GHz and up to 100 Gbit/s across multiple bands[10]. The device-level trade-offs of these MUTC implementations are discussed in Section 1.4.

System-level results further broaden the design space. A full-photonic-conversion D-band bridge achieved a 123.72-Gbit/s net rate over 10 km fiber, 0.6 m wireless, and 5 km fiber[33]. An all-plasmonic 285-GHz link reached a 111.7-Gbit/s achievable information rate over 5 m[18], and a minimalist integrated photonic transceiver supported 144 Gbit/s at 200 GHz over 20 cm[16]. At higher capacity, a 322-GHz MIMO system reported 510 Gbit/s with embedded adaptive phase recovery[34]. At the opposite distance extreme, photonics-aided transmission was extended to 20.1 km through link engineering and neural-network equalization[35]. Together, these experiments illustrate complementary progress in photonic integration, fiber-wireless conversion, spatial multiplexing, digital signal processing, and transmission reach. Carrier frequency and per-antenna data rate alone do not capture system-level differences in wireless reach, fiber span, device integration, conversion architecture, and digital signal processing.

Figure 5 links the photonic parallelization mechanism to the measured system capacity. As shown in Figure 5(a), an optical local-oscillator tone and two modulated optical carriers are combined in the optical domain and delivered to X- and Y-polarization photomixing branches. The combination of wavelength- and polarization-division multiplexing therefore provides four parallel THz channels. Figure 5(b) shows the corresponding measured line rates of 155.01, 146.63, 159.81, and 151.20 Gbit/s after 2.8 m transmission at 320 – 380

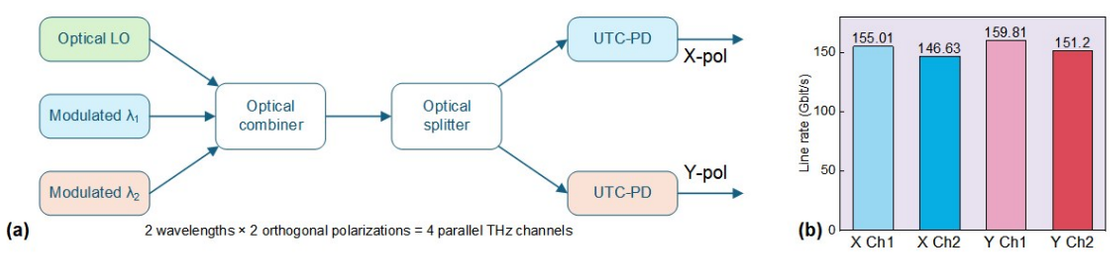

Fig. 5 Photonic parallelization and measured capacity of a 320 – 380 GHz THz link: (a) four parallel channels enabled by optical-domain WDM and dual-polarization photomixing; (b) measured channel rates after 2.8 m wireless transmission. Redrawn using the architecture and measured data reported in Ref. [29]
图5 320~380 GHz太赫兹链路的光子并行传输与实测容量:(a)采用光域波分复用和双偏振光混频实现的四路并行信道;(b)经过2.8 m无线传输后的各信道实测速率。根据文献[29]报道的系统架构和实测数据重绘。

GHz. The resulting aggregate line and net rates were 612.65 and 510.5 Gbit/s, respectively, with an average net spectral efficiency of 4.445 bit/s/Hz per polarization[29].

Table 1 therefore complements Figure 4 by summarizing representative photonics-assisted experiments across these additional dimensions[8-10,12-14,16,18,33-35].

These demonstrations represent different operating points; gross and net rates, aggregation, reach, and processing conditions must be distinguished before comparing architectures.

1.3 Photonic carrier generation and OE/EO conversion

The OE conversion generates mmWave or THz signals through multi-tone light generation and photonic mixing. The frequency interval between the optical tones determines the center frequency of the mmWave or THz signal, while the bandwidth of the photonic mixer determines the available radio-frequency band. Multi-tone light sources can be generated using free-running laser diodes (LDs) or optical frequency combs. Free-running LDs provide a simple multi-tone source, but their frequency drift directly affects the generated carrier. For multi-antenna links, an optical frequency comb generates multiple wavelengths with adjustable and uniform frequency intervals, thereby maintaining the frequencies of the transmitted signals. Integrated optical frequency division and injection-locked dual-laser chips provide additional options for low-noise and compact carrier generation[8,11,36-38].

Photonic mixers operate differently from electrical mixers. An electrical mixer multiplies the baseband signal by a carrier generated by an electronic local oscillator to produce the mmWave or THz signal. By contrast, a photonic mixer commonly uses a photodiode to convert optical power into an electrical current. Through square-law detection, the optical wavelength components beat with each other, generating a mmWave or THz signal at their difference frequency.

EO conversion uses ultra-wideband optical modulators to directly modulate a received radio signal onto an optical carrier, thereby transferring the mmWave or THz waveform to the optical domain for subsequent coherent detection. Depending on the required bandwidth, the receiving modulator can be a Mach - Zehnder modulator (MZM) or a phase modulator (PM)[19,27,39]. The modulated optical signal is subsequently detected by a coherent receiver, which provides higher sensitivity and capacity than intensity-modulation/direct-detection systems. Full photonic down-conversion has also progressed beyond a conceptual receiver-side option. Thin-film lithium niobate modulators and plasmonic or graphene electro-optic interfaces have been investigated for compact mmWave/THz-to-optical conversion[10,15-17,33,40-41]. Thin-film lithium niobate modulators with bandwidths beyond 100 GHz have enabled W-band photonic down-conversion[26], while plasmonic electro-optic modulators operating from 500 GHz to 2.5 THz have extended microwave-photonic conversion into the sub-THz and THz ranges[31].

Table 2 compares receiver conversion paths according to the source of the local oscillator and the location of frequency conversion.

Electronic receive mixers may use either electronic or photonically generated local oscillators. A receiver using a photonically generated LO to drive an electronic mixer is demonstrated in Ref. [42]. Direct photonic downconversion is attractive when broad RF bandwidth or transparent optical forwarding is required, particularly

Table 1 Representative system-level photonics-assisted wireless experiments with different integration, conversion, and transmission configurations
表1 不同集成、光电转换和传输配置的代表性系统级光子辅助无线实验

Example	Reported results	Technical significance
Integrated dual-laser photonic chip[8]	408 GHz carrier; 131.21 Gbit/s net rate over 10.7 m.	Integrated high-purity carrier generation for ultrafast THz wireless.
Graphene optoelectronic mixer[9]	More than 96 GHz optoelectronic bandwidth; 93 GHz 4 Gbit/s link.	Compact optoelectronic mixing with a remaining conversion-efficiency limitation.
TFLN on-chip wireless photonics[10]	0.5-115 GHz tunable operation and up to 100 Gbit/s transmission across multiple bands.	Integrated reconfigurable operation over an exceptionally broad frequency range.
MUTC photodiode modules[12-14]	206 GHz device bandwidth; 120 Gbit/s at 150 GHz over 54 m; D-band 160 Gbit/s module-level link.	Module-level progress in output power, bandwidth, and responsivity.
Full photonic conversion[33]	123.72 Gbit/s net data rate over 10 km fiber + 0.6 m wireless + 5 km fiber.	Complete fiber-wireless-fiber conversion architecture.
All-plasmonic link[18]	285 GHz; 111.7 Gbit/s achievable information rate over 5 m.	Compact optical-THz-optical interface beyond conventional UTC-PD transmitters.
Integrated minimalist transceiver[16]	200 GHz; 144 Gbit/s over 20 cm.	Compact coherent generation and reception with simplified phase tracking.
High-capacity MIMO[34]	322 GHz; 510 Gbit/s with embedded adaptive phase recovery.	Capacity benefit and DSP burden of spatial multiplexing.
Long-distance photonic-assisted link[35]	20.1 km wireless reach with neural-network equalization.	Propagation engineering and DSP optimized for reach rather than peak rate.

Table 2 Comparison of receiver conversion paths and operating considerations
表2 接收变频路径及工作条件比较

Architecture	Signal path	Suitable applications	Main considerations
Electronic downconversion	Received RF → electronic mixer driven by an electronic LO → IF/baseband	Compact receivers where electronic circuits meet the required bandwidth and sensitivity	Mixer conversion loss and noise, LO bandwidth and phase noise, and RF-chain power consumption
Hybrid reception with a photonic LO	Optical tones → photomixer → RF LO; received RF → electronic mixer → IF/baseband	Systems requiring tunable LO generation, optical LO distribution, or reference sharing	Electronic mixer bandwidth and noise; optical-source, photomixing, distribution, and stabilization requirements
Electronic downconversion with optical IF transport	Received RF → electronic mixer → IF → optical transport → centralized detection/DSP	Fiber-connected receivers with centralized processing	Optical IF conversion and transport add loss, noise, and power consumption; RF downconversion remains electronic
Direct photonic downconversion	Received RF → EO modulation → optical coherent detection → IF/baseband	Broadband conversion or transparent fiber–wireless–fiber forwarding	EO drive requirements, optical insertion loss, laser and amplifier noise, and coherent-receiver power; RF preamplification may be required

where optical sources and processing resources can be shared. Its sensitivity and energy performance depend on the RF power needed to drive the EO interface, any preceding amplification, optical insertion loss, laser and amplifier noise, and subsequent coherent detection. If an electronic receiver already meets the bandwidth and sensitivity requirements, additional optical conversion may offer little benefit. Ref. [33] illustrates direct photonic conversion with electronic RF amplification; "direct" describes the conversion path rather than the absence of electronics. The gain in frequency agility must be weighed against phase coherence, conversion loss, and the power required for optical amplification and stabilization.

Figure 6(a) illustrates the wide frequency agility of a TFLN wireless-photonic platform by comparing the measured line rates of QPSK and 16-QAM signals at ten carrier frequencies. A single integrated platform generated signals from 0.5 to 115 GHz, while communication was experimentally verified in the 10–45 and 85–100 GHz ranges. The 16-QAM line rate reached 100 Gbit/s at both 35 and 95 GHz[10]. The result demonstrates that the same photonic conversion platform can support reconfigurable operation across microwave, mmWave, and sub-THz bands.

1.4 Optoelectronic devices and integrated interfaces

Key optoelectronic devices perform optical-to-mmWave/THz and mmWave/THz-to-optical conversion[19,26-27]. Among the available approaches, photodiode-based photonic mixers are compatible with existing optical-fiber networks and facilitate fiber-wireless integration in 6G RANs. Through optical heterodyne detection in the photodiode, photonics-assisted transmitters simultaneously realize optical-to-electrical conversion and baseband-to-radio-frequency up-conversion.

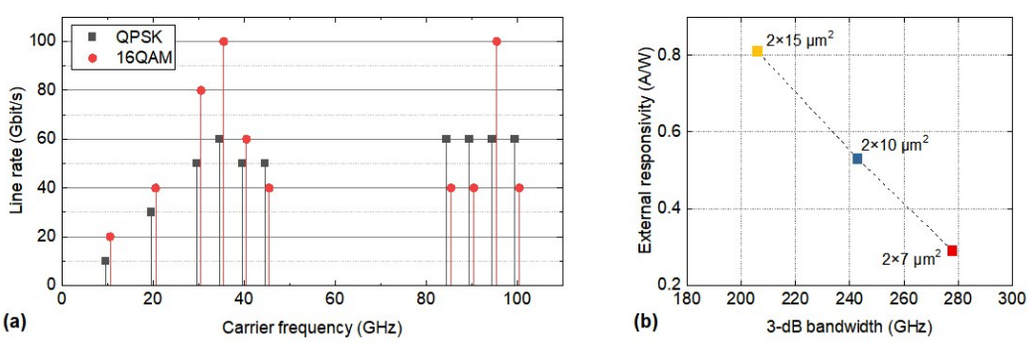

Fig. 6 Broadband photonic conversion and MUTC-PD performance: (a) measured TFLN data rates over 10-45 GHz and 85-100 GHz; (b) MUTC-PD bandwidth and responsivity. Redrawn from Refs. [10,12]
图6 宽带光子转换与MUTC光电探测器性能:(a)TFLN平台在10-45, 85-100 GHz范围内的实测速率;(b)MUTC光电探测器的带宽和响应度。根据文献[10,12]重绘

The two most established types of PDs commonly used for fiber-wireless integrated mmWave and THz RAN are the PIN-PD and UTC-PD[19,26-27]. PIN-PDs are mature components in optical-fiber systems, whereas UTC-PDs and MUTC-PDs are specifically optimized for higher bandwidth and output power in mmWave and sub-THz photomixing[19,26-27,43]. The operating principles and evolution of UTC photodiodes are reviewed in Ref. [43], and antenna-integrated photonic arrays are demonstrated in Ref. [44]. Broadband lithium-niobate modulators and hybrid silicon – lithium-niobate interfaces are reported in Refs. [45-46].

UTC-PDs remain central, but recent modified UTC photodiodes have pushed the discussion toward module-level power, bandwidth, and responsivity. Representative MUTC results include a high-power F-band module for beyond-100 Gbit/s wireless sub-THz links[14], a D-band module for 160 Gbit/s photonics-assisted fiber-THz integration[13], and a 206 GHz-bandwidth device with 0.81 A/W external responsivity supporting 120 Gbit/s at 150 GHz over 54 m without a low-noise amplifier (LNA)[12]. These results demonstrate progress from device-level bandwidth toward module-level power, responsivity, and link reach. Figure 6(b) compares MUTC-PDs with active areas of 2×7, 2×10, and 2×15 μm^2. Their measured 3-dB bandwidths were 278, 243, and 206 GHz, with external responsivities of approximately 0.29, 0.53, and 0.81 A/W, respectively[12]. These results show the bandwidth – responsivity trade-off of the photonic-to-THz interface.

No single device platform simultaneously maximizes bandwidth, output power, conversion efficiency, and compactness. UTC and MUTC photodiodes remain central to optical-to-mmWave/THz conversion because of their high speed and useful output power. Thin-film lithium niobate supports broadband and reconfigurable electro-optic conversion[10,15,45-46]. Plasmonic interfaces provide strong field confinement and compact optical-THz-optical conversion[18,31,41], while graphene devices offer broadband mixing and reception in a small footprint[9,17]. Integrated lasers and optical frequency-division platforms improve carrier coherence and reference sharing[8,11]. These platforms provide complementary functions within photonics-assisted transmitters and receivers. Device selection should use the linear RF power and bandwidth available after coupling and packaging.

1.5 Waveform design, modulation formats, and coherent DSP

The approach to the upper limit of spectral efficiency has also been a topic of study. Figure 7 illustrates representative waveform-design approaches for improving spectral efficiency. Single-carrier modulation (SCM) is relatively simple, and pulse shaping controls occupied bandwidth and inter-symbol interference. Multicarrier waveforms such as orthogonal frequency-division multiplexing (OFDM) support flexible sub-band allocation, while orthogonal time-frequency space (OTFS) maps information in the delay-Doppler domain. Faster-than-Nyquist (FTN) signaling intentionally introduces controlled inter-symbol interference by reducing symbol spacing, with sequence detection or equalization used for recovery. Various ways have been proposed to synthesize the spectrally efficient signals, i. e., using narrow-band linear filtering and finding the optimal signal shape by solving the optimization problem. Related W- and D-band demonstrations using high-order modulation, bidirectional radio-over-fiber (RoF), and learning-assisted equalization are reported in Refs. [47-49].

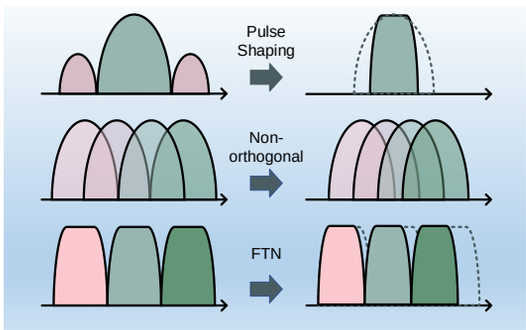

Fig. 7 Advanced waveform design for 6G
图 7 面向6G的先进波形设计

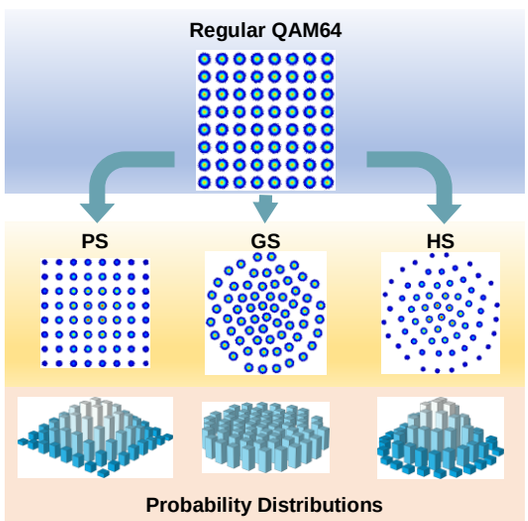

Fig. 8 Advanced modulation formats with constellation probabilistic shaping, geometric shaping, and hybrid shaping
图 8 具有星座概率整形、几何整形和混合整形的先进调制格式

In addition to waveform design, Figure 8 shows that constellation shaping has proved to be a useful technology offering a signal-to-noise ratio (SNR) gain up to the ultimate shaping gain of 1.53 dB. Two typical ways can be used to obtain the shaping gain, probabilistic shaping (PS) and geometric shaping (GS). PS designs symbol probabilities to approximate the Maxwell-Boltzmann distributions, allowing them to operate close to the AWGN capacity. The signal entropy can be adapted to the channel capacity by changing different probabilistic distributions[19]. Unlike the probabilistic shaping in which the constellation is still on a uniform grid with differing prob-

abilities per constellation point, in GS, the constellations are usually designed in various non-square shapes. Compared with the uniform quadrature amplitude modulation (QAM), the points in the GS constellation have a larger Euclidean distance, so the signal can have a larger average power and SNR at the same peak-to-peak value in time-domain modulations. Both approaches increase SNR gains by optimizing the shape of the constellation in two different dimensions. In the pursuit of extreme performance, the combination of PS and GS has been proposed. PS provides flexible entropy adaptation, whereas GS improves the Euclidean-distance distribution of the constellation. Hybrid shaping combines these two advantages. Hybrid shaping (HS) leverages the advantages of these two technologies, adjusting the distribution points based on the GS constellation. In fiber-wireless cascades, the signal-processing design consequently depends on impairments from both the optical and wireless channels.

In the preceding discussion, the advanced modulation formats and waveform design at the transmitter side are used to raise the spectrum efficiency and improve the transmission performance. For a coherent detection system, advanced coherent DSP algorithms at the receiver side will be further required to enhance the sensitivity of the receiver and the system capacity[50]. Coherent detection is suitable for both SCM and OFDM signals, corresponding to different DSP algorithms[50].

DSP has become an integral part of the transceiver architecture. Phase-noise and carrier-frequency-offset estimation are required when optical heterodyning, laser linewidth, and high-order QAM interact. Linear frequency-domain equalization compensates bandwidth limitation and frequency-selective fading, whereas Volterra and learning-based equalizers address nonlinearities introduced by photodiodes, modulators, amplifiers, and fiber-wireless channels. Adaptive Kramers-Kronig reception has been combined with probabilistic shaping in D-band fiber-THz systems[51]. MIMO links additionally require channel separation, phase alignment, and adaptive phase recovery, as illustrated by the 322-GHz 510-Gbit/s experiment[34], while neural equalization has supported multi-kilometer demonstrations[35,52]. End-to-end learning provides an additional optimization framework, subject to the data, generalization and implementation conditions discussed in Section 3.3[53-54]. A waveform is useful only if its net-throughput gain survives the required backoff, equalization latency, and real-time processing power.

1.6 Multidimensional multiplexing for capacity scaling

Fiber-wireless integration supports multidimensional multiplexing across baseband, optical-fiber, and wireless domains[55]. Each additional wavelength, polarization, spatial mode, antenna, or frequency band can create a parallel channel, subject to crosstalk, hardware complexity, and DSP overhead. As more dimensions are combined, the capacity of the system with high-density radio access cells can be increased significantly. As shown in Figure 9, various multiplexing methods can be realized in digital baseband signal generation, fiber optic transmission, and wireless transmission.

In fiber optic transmission links, multidimensional multiplexing methods mainly include frequency division multiplexing (FDM) or wavelength division multiplexing (WDM), polarization division multiplexing (PDM), and space division multiplexing (SDM). FDM is mainly used in the generation of the baseband signal by digital carrier modulation technologies, such as OFDM and multi-band SCM. A WDM system modulates the electrical signals to optical carriers of different wavelengths. These optical signals can be separated by optical filters. PDM utilizes the orthogonality of horizontal and vertical polarization. In addition, multi-mode fiber (MMF) and multi-core fibers (MCFs) can be used in fiber optic communication to achieve SDM[56]. Mode and core multiplexing can be used simultaneously in an MCF to further increase the multiplexing depth.

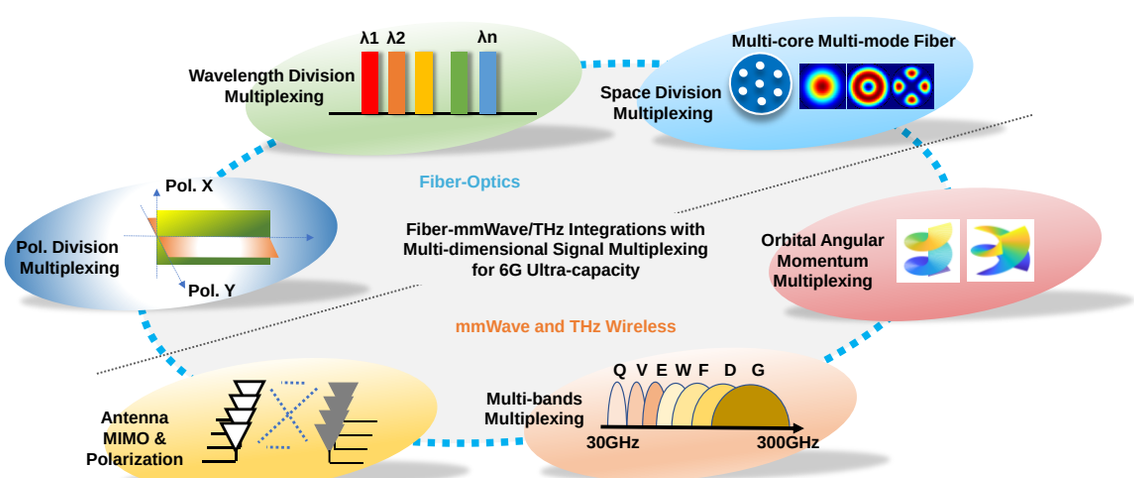

Fig. 9 Multidimensional multiplexing for 6G ultra-high-capacity: wavelength, polarization, and space in fiber, antenna, frequency-band, and OAM in wireless

图 9 面向6G超大容量通信的多维复用:光纤中的波长、偏振与空间复用,以及无线链路中的天线、频带与轨道角动量(OAM)复用

In mmWave and THz wireless links, antenna multiplexing, multiband multiplexing, and orbital angular momentum (OAM) multiplexing can further extend the system capacity in the air interface[57]. Low-frequency dual- or three-polarization antennas are commercially available. However, high-frequency W-band polarization antennas are challenging to design but are studied intensively. Antenna arrays with multi-input and multi-output (MIMO) can take advantage of a smaller footprint and higher gain in high frequency compared with low-frequency waves. OAM can provide a set of orthogonal modes on the same frequency channel, which is different from the conventional multiplexing methods[57]. Additional channels increase useful capacity only when crosstalk, optical splitting loss, calibration, and DSP overhead do not consume the corresponding gain.

2 Challenges of photonics-assisted mmWave and THz 6G systems

2.1 Link budget and photonic conversion efficiency

The propagation of mmWave and THz signals is different from that of lower frequency signals. The differences bring both challenges and opportunities for system design. mmWave and THz signals experience substantial path loss, which restricts RRU coverage[3]. The resulting reduction in cell radius leads to a denser RRU topology for continuous coverage. High propagation loss further requires a large link budget. Transmit power is a major determinant of mmWave and THz transmission distance[25]. Output power and baseband-to-radio conversion efficiency are also key constraints on the achievable transmission distance. For a photonic transmitter, the radio link budget also includes the optical power launched into the photomixer, photodiode responsivity and saturation, O/E conversion efficiency, optical insertion and coupling loss, and the efficiency of the antenna or waveguide interface.

Table 3 compares representative D-band implementations under their reported operating conditions. Saturated output power, linear modulated power, responsivity, and conversion efficiency describe different aspects of performance. Device bandwidth should also be distinguished from the usable signal bandwidth after packaging. For photonic generation, the optical-to-RF conversion efficiency, $\eta_{O/RF} = P_{RF,out}/P_{opt,in}$, differs from the transmitter wall-plug efficiency, $\eta_{wall,Tx} = P_{RF,out}/P_{elec.,Tx}$. The latter includes the electrical power consumed by the transmitter optical sources, amplifiers, drivers, bias circuits, and thermal control. Both quantities should be evaluated at a specified operating point with defined input and output reference planes. Receiver power is included separately in the full-link energy budget discussed in Section 2.6.

To illustrate the effect of RF output power, consider a 140-GHz link over 10 m with transmit and receive antenna gains of 25 dBi each and an additional loss of 3 dB. The free-space path loss is 95.37 dB, giving received powers of −53.37 and −43.37 dBm for assumed linear transmit powers of −5 and +5 dBm, respectively. At approximately 290 K, a 10-GHz receive noise bandwidth and a 10-dB noise figure give a noise floor of −64 dBm. A required SNR of 20 dB therefore corresponds to a receive-power threshold of −44 dBm and link margins of −9.37 and +0.63 dB. This calculation uses a common set of assumptions to show the effect of launch power; it does not represent a measured comparison of the implementations in Table 3. Practical budgets should also account for frequency-dependent absorption, alignment and implementation losses.

2.2 Device bandwidth, saturation, packaging, and conversion constraints

A larger nominal spectrum does not automatically produce higher capacity. The useful bandwidth is jointly limited by light-source phase noise, modulator bandwidth, photodiode saturation, antenna gain, waveguide and package loss, data-converter bandwidth, and digital signal processing. These coupled limitations determine the effective bandwidth and achievable information rate of the complete link. The remaining issues include conversion efficiency, optical insertion loss, bias stability, receiver noise, and real-time coherent processing. The available conversion range is ultimately limited by the electro-optic bandwidth of the receiving modulator and

Table 3 Comparison of representative D-band implementations
表3 代表性D-band实现方案的指标比较

Implementation	Reported metrics	Measurement conditions
Electronic CMOS transmitter, 140 GHz[58]	Saturated output power: 10.1 dBm; output 1-dB compression point: 6.5 dBm; DC power: 435 mW; 3-dB bandwidth: 5.5 – 6.1 GHz	On-wafer transmitter measurements. The DC power covers the two-channel transmitter chip.
MUTC photonic transmitter[12]	Device bandwidth: 206 GHz; external responsivity: 0.81 A/W; packaged RF output: > −5 dBm over 127 – 185 GHz; transmission: 120 Gbit/s over 54 m at 150 GHz	Device bandwidth and packaged output power are reported separately from the transmission result. The module operating range extends beyond the 170-GHz upper boundary of D-band.
Full-photonic bridge, 123 GHz[33]	Net rate: 123.72 Gbit/s; transmission distance: 10 km fiber + 0.6 m wireless + 5 km fiber; photomixer responsivity: 0.05 A/W; saturation photocurrent: 7.5 mA at 120 GHz	The link includes RF receive amplification and optical amplification. Saturation photocurrent was characterized at 120 GHz.

the bandwidths of the associated electronic and passive components.

At D-band frequencies and above, package parasitics and RF transitions can substantially reduce the bandwidth measured at device level. Co-design of photonic devices, RF interfaces, antennas, bias circuits, and thermal control is therefore required. For UTC and MUTC photodiodes, saturation, heat removal, impedance matching, and antenna or waveguide coupling determine module performance[12-14].

The UTC-PD and antenna must be optimized as a coupled RF source – load system. For a linear Thevenin representation with positive source and load resistance and impedances Z_{PD} and Z_A, the mismatch power-transfer factor is $\eta_m = 4\mathrm{Re}(Z_{PD})\mathrm{Re}(Z_A)/|Z_{PD}+Z_A|^2$. This factor refers to available source power and excludes radiation loss. Conjugate matching maximizes it at one frequency, but a narrow resonance can reduce the usable modulation bandwidth. Junction capacitance, carrier transit time, bias, photocurrent, interconnect parasitics, and thermal limits must therefore be evaluated together with antenna radiation efficiency. In a tightly coupled array, the relevant load is the scan-dependent active impedance, including mutual coupling. For an antenna-coupled EO receiver, the corresponding objective is efficient RF-field overlap and voltage delivery to the modulation region, while controlling loss and noise. Improving matching alone cannot remove photodiode saturation or optical-to-RF conversion losses[12-14,43-44].

2.3 Carrier coherence and receiver impairments

Optical frequency division and injection-locked dual-laser schemes reduce phase-noise penalties and support shared coherent references, but they impose additional constraints on thermal control, locking range, packaging, and manufacturability. Laser linewidth contributes carrier phase noise and therefore affects coherent-detection sensitivity and phase-recovery complexity[50]. A large linewidth introduces phase noise to the signal. Therefore, it also raises interest in performance analysis in photonics-assisted mmWave and THz communication systems. Figure 10 shows the simulated sensitivity penalty as a function of the combined linewidth-symbol-duration product for 25-GBaud 64QAM signals using different transceiver architectures. The simulation results show that the optical transmitter with electronic receiver (OTER) and electronic transmitter with optical receiver (ETOR) architectures have the same tolerance to the combined linewidth-symbol-duration product. The performance of the optical transmitter with optical receiver (OTOR) architecture is more sensitive to the linewidth since it has two optical beating and detection stages during the fiber-wireless-fiber conversions. As the linewidth of the lasers increases, the sensitivity penalty increases because of the induced phase noise.

2.4 Wideband waveform and real-time DSP complexity

Although spectrum resources in the mmWave and THz bands are abundant, the bandwidth of the components is limited. The physical layers of mmWave and

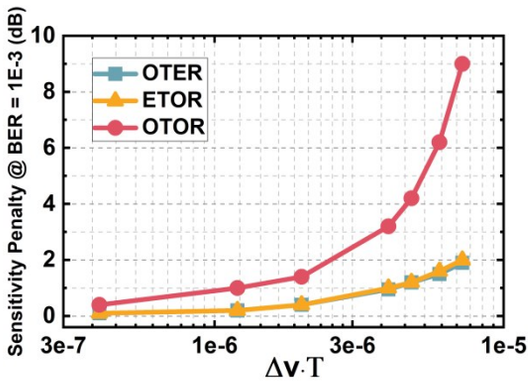

Fig. 10 Sensitivity penalty versus combined linewidth-symbol-duration product for 25-GBaud signals with different transceiver architectures. (Δv: the full width at half maximum of the LD emitting spectrum (Hz), T: the duration time of a symbol (s))
图 10 不同收发机架构下25 GBaud信号的灵敏度代价与联合线宽—符号持续时间乘积的关系(Δv:激光二极管发射光谱的半峰全宽,单位为Hz;T:符号持续时间,单位为s)

THz systems need novel waveform design and modulation schemes considering the constraints of the practical systems[19,26-27]. Non-orthogonal waveforms introduce inter-symbol interference (ISI), and the corresponding equalizer must compensate for the combined optical and wireless transfer functions.

The DSP burden in a photonics-assisted link is determined by the cascaded optical, radio-frequency, and wireless transfer functions rather than by the wireless channel alone. Optical heterodyne phase noise, modulator nonlinearity, photodiode saturation, frequency-selective RF responses, and multipath fading may coexist within the same bandwidth. OFDM and multiband waveforms permit sub-band equalization and adaptive bit loading, but their peak-to-average power ratio increases the operating back-off of modulators, photodiodes, and RF amplifiers. Frequency-domain, Volterra, Kramers – Kronig, and learning-based equalizers have been demonstrated across W-band, D-band, and higher-frequency photonics-assisted links[25,34-35,47-52,59].

Real-time implementation introduces constraints not represented by offline-DSP line-rate records. Processing load scales with sampling rate, quantization resolution, equalizer memory, transform size, spatial-channel count, and iterative updates. Synchronization, channel estimation, frequency-offset compensation, carrier-phase recovery, MIMO separation, and forward-error correction also contribute to latency. Parallel hardware raises throughput, whereas high-speed data conversion and data movement add power consumption. Comparison across demonstrations depends on net throughput, sampling conditions, numerical precision, latency, and processing platform[19,34,50-52].

2.5 Beam control and multi-antenna scaling

In addition, mmWave and THz signals are highly directional and behave more like narrow optical beams than lower-frequency radio links[3]. The mmWave and THz signals have poor non-line-of-sight (NLOS) propagation ability due to high reflection loss. The active manipula-

tion of the beam will enhance the system's performance. Thus, the beamforming technique is essential for application in complex environments.

Looking toward 6G, aggregate mmWave and THz systems are expected to support data rates beyond 1 Tbit/s[1]. It is challenging to meet this requirement within a single link. The use of multiplexing dimensions, such as polarization, space, and mode, can increase the aggregate data rate and expand the capacity of mmWave and THz systems. The OAM generation, OAM antenna alignment, and OAM signal reception are still major challenges before OAM can be commercially available on a large scale.

In a photonics-assisted array, capacity scaling also requires additional optical tones, modulators or photodiodes, package interfaces, coherent references, calibration, and DSP resources for each antenna or spatial channel.

2.6 Integration platforms, energy efficiency, and manufacturability

System-level integration must combine light sources, modulators, photodiodes, RF circuits, antennas, packaging, thermal control, and signal processing. The resulting energy consumption includes laser and optical-amplifier power, bias and thermal-control power, RF amplification, data conversion, and DSP. Heterogeneous integration therefore remains constrained by coupling loss, process compatibility, yield, channel-to-channel variation, calibration, reliability, and cost.

Table 4 compares the functions, integration requirements, power considerations, and manufacturing implications of representative photonic platforms[8-18,39,43,45-46,60].

Each platform should be selected according to the function it performs. A practical architecture can combine III – V sources and photodiodes, low-loss optical routing, broadband EO modulation, and electronic amplification and control. An InP UTC-PD heterogeneously integrated with a TFLN modulator illustrates this approach[60]. The photodetector provides a bandwidth of 240 GHz, with internal and external responsivities of 0.67 and 0.21 A/W, respectively. At the module level, optical mode matching, thermal compatibility, bonding yield, RF transitions, and packaged reliability must be considered together. CMOS-compatible fabrication of an individual photonic component does not mean that the complete heterogeneous THz transceiver can be manufactured in an unmodified CMOS process.

System-level energy per delivered bit is $E_b = P_{total}/R_{delivered}$, where P_{total} is the electrical power consumed at both link ends and $R_{delivered}$ is the successfully delivered payload rate after coding, protocol and retransmission overheads. The power budget includes optical sources and amplifiers, RF circuits, modulator drivers, bias and thermal control, ADCs/DACs, DSP/FEC, and control functions. Electronic downconversion requires the electronic LO and mixer chain; a photonic LO additionally requires optical generation, distribution and stabilization; direct photonic conversion requires the EO interface and optical receiver. Optical and radiated powers are outputs of this electrical budget and should not be counted again.

Ref. [16] reports receiver power estimates of 4.84 W for conventional coherent reception and 2.89 W for residual-carrier/injection-locking reception at a line rate of 144 Gbit/s, corresponding to 33.6 and 20.1 pJ per line bit. These estimates include lasers, photodetectors, TIAs and DSP modeled for 7-nm CMOS; ADC, FEC, thermal control and transmitter power are outside the reported sum. The comparison therefore describes receiver energy per line bit, with a different accounting boundary from full-link energy per delivered bit.

For N equally loaded links, total power can be written as $P_{total}(N) = P_{shared}(N) + NP_{branch}(N)$. Relative to a reference consuming P_{ref} per link at the same delivered rate and link quality, resource sharing saves power when $P_{shared}(N) < N\left[P_{ref} - P_{branch}(N)\right]$. Optical splitting loss, stabilization requirements and processing load can increase both the shared and branch terms as the network expands. This condition links the benefit of centralized

Table 4 Integration platforms and implementation considerations
表4 集成平台与实现条件

Platform and function	Process and compatibility	Power and loss considerations	Manufacturing and cost considerations
III – V: lasers and UTC/MUTC photodiodes	Provides optical gain and absorption; integration with silicon or TFLN requires bonding, transfer, or co-packaging	Laser electrical power, photodiode bias, saturation, and heat removal	Established device processes; module cost and yield depend on assembly, coupling, and thermal management
Silicon photonics: optical routing, modulation, and control interfaces	Supports foundry fabrication; efficient light sources generally require external or heterogeneously integrated III – V devices	Modulator drive power, insertion loss, and thermal-tuning power	Wafer-scale fabrication supports volume production; packaging, testing, and light sources remain important cost factors
TFLN: broadband EO conversion	Requires low-loss waveguides, RF electrodes, optical transitions, and integration with sources and photodiodes	Modulation efficiency, optical insertion loss, bias control, and RF-drive power	Cost depends on wafer processing, optical coupling, bonding, and packaged yield
Plasmonic and graphene interfaces	Supports compact field confinement or broadband mixing, depending on the device; integration requirements vary by process	Optical loss, conversion efficiency, operating stability, and required optical/RF power	Process uniformity, packaging, and long-term reliability require further development

resources to the incremental power required by each additional link.

3 Future Prospects

3.1 Photonic coupled antenna arrays

The antenna is an essential component in the photonics-assisted mmWave and THz generation and reception. It will be important in future photonics-assisted mmWave and THz communication systems for 6G RANs. With the development of the 6G access network with high-throughput mobile communications, ultra-wideband array antennas that have a low profile and wide beam steering range are required for broadband beam steering. As a result, the tightly coupled array (TCA) antenna has attracted increasing research interest recently owing to its extremely wide frequency range. The photonics TCA with high-power UTC-PD, serving as the current source for exciting a coupled-dipole element, is also reported to overcome the limitations of electronic feed networks for mmWave phased arrays[44]. Charge-compensated (CC)-MUTC photodiodes were integrated with the dipole array by sequential flip-chip bonding[44].

A similar structure can also be used at the receiver side in the mmWave/THz-to-optical conversion process for the photonic down-conversion. For example, the antenna-coupled-electrode (ACE) electro-optic modulators where an array of ACEs is set along the optical waveguide have been demonstrated to convert wireless W-band mmWave signals into optical signals. Therefore, ACE electro-optic modulators provide a potential receiver-side conversion approach in future fiber-wireless integrated mmWave and THz 6G RAN with little distortion and reduced coupling loss. These arrays therefore require the impedance, bandwidth, and thermal co-design discussed in Section 2.2; the optimization target is radiated signal power or receive conversion sensitivity over the operating band and scan range.

3.2 Novel photonic beamforming technologies

In 6G mmWave and THz systems, beamforming supports resource allocation and link optimization for the access segments. Phase control units (PCU) and true time delay (TTD) are the basic components in the generation of beamforming signals. Both electronic integrated circuit (EIC) and photonic integrated circuit (PIC) approaches to mmWave beam steering suffer from bandwidth limitations and high insertion loss[61]. As frequency increases into the mmWave and THz bands, frequency-dependent loss increasingly limits EIC approaches, while optical delay networks can exhibit substantially weaker RF-frequency dependence than electronic feed networks, although modulator, detector, and packaging responses remain bandwidth-limited. However, the integration technology for PIC is still under development. The integration of large array delays realized in PIC and sub-array delays realized in EIC provides a potential hybrid solution[61].

Another important approach to beam control in 6G mmWave and THz systems is the reconfigurable intelligent surface (RIS). RIS offers the concept of smart radio environment, manipulates beams by reflecting or passing through, and supports NLOS communication[3,62]. With fiber-wireless integrated RAN, it is possible to provide a distributed deployment of signal flows in a "line or wire"-like network by cascading photonics-assisted mmWave and THz links with RISs[1]. The breakthroughs in the manufacturing of RIS, the configurable material, and the compatible interface will expand the RIS applications[62].

For broadband 6G links, photonic true-time-delay networks can mitigate the beam squint of phase-shifter arrays by providing frequency-independent delay. A realistic architecture may combine PIC-based large-array delay, EIC-based subarray control, and antenna-in-package integration[63-65].

For broadband beamforming, the next step is to demonstrate steering range and residual beam squint together with delay range, delay error, optical loss, calibration time, and control power. A hybrid PIC/EIC partition is useful only when its wideband beam-control benefit exceeds the additional interfaces and stabilization burden [61,63].

3.3 AI-assisted and end-to-end optimization

Learning-based optimization is useful when measured nonlinear or coupled impairments are difficult to represent with a compact analytical model. It should be compared with linear equalization, phase recovery, Volterra processing, and model-based adaptation at the same net rate, error criterion, latency, and power budget. For stable channels dominated by linear distortion or well-characterized phase noise, conventional DSP may provide a simpler and more predictable solution. The long-distance examples in Refs. [52, 66] should also be distinguished: Ref. [52] uses a neural equalizer, whereas Ref. [66] demonstrates SIMO/MRC diversity and is not evidence of neural equalization.

Native AI provides a potential approach to automating the optimization and management of complex 6G-oriented fiber-wireless systems. It enables end-to-end optimization of the physical layer through learning-based methods. Figure 11 shows that the resemblance of the communication system to a deep neural network (DNN) can be utilized to interpret the entire communication system as an autoencoder (AE) so that the transmitter and receiver can be jointly optimized. The AE contains a network layer as the digital twin to simulate and describe the states, behaviors, and rules for the combinations of hardware and channel impairments.

Training data should cover the relevant carrier frequencies, optical powers, bias points, temperatures, phase noise, blockage and channel conditions, using measured pilot or labeled sequences together with a validated physical model. Validation should separate acquisition sessions and hardware conditions to test generalization rather than only random samples from one recording. Online use requires inference and update latency to fit the adaptation budget; FPGA or ASIC acceleration, quantization, pruning, and memory traffic must be considered at the target sampling rate. End-to-end learning additionally requires a validated differentiable surrogate

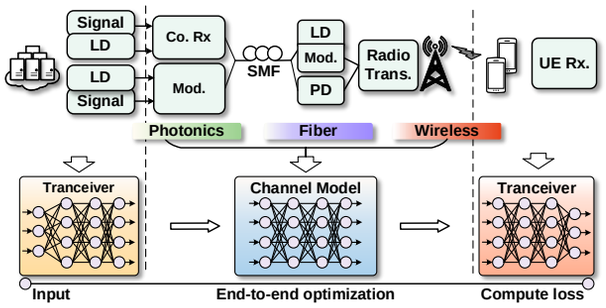

Fig. 11 End-to-end learning in photonics-assisted mmWave and THz 6G system
图 11 光子辅助毫米波与太赫兹 6G 系统中的端到端学习

or a hardware-compatible optimization method. Model mismatch, retraining overhead, and training energy must be included in the assessment. A conventional-DSP fallback is appropriate when drift or limited data invalidates the learned model[52-54].

3.4 Integrated sensing and communication in photonics-assisted mmWave and THz 6G systems

Potential 6G applications include smart cities, smart homes, smart healthcare, and vehicle-to-everything (V2X), in which sensing will play an important role. Integrated sensing and communication (ISAC) can alleviate competition for spectrum resources by allowing communication and sensing functions to share waveforms, hardware, and signal-processing resources, and provide integration and collaboration benefits for the system.

This also means that in 6G, nodes on each network will have the ability to be intelligent and aware of their surroundings, and can share the results of these observations through communication capabilities. Efficiently integrating sensing and communication in photonics-assisted mmWave and THz systems remains an important research topic. Figure 12 illustrates a fiber-wireless ISAC architecture in which sensing and communication signals are centrally processed and distributed to multiple photonics-assisted mmWave/THz base stations.

Photonics-assisted mmWave and THz systems offer large signal bandwidths that can improve the sensing resolution as well as communication speed. They also support distributed networking over optical fiber, which helps to improve the coordination of sensing and communication processing and increase the coverage area. In the field of radar sensing, many studies have used microwave photonics-assisted methods to achieve better performance in terms of resolution, coverage, and speed[67]. Therefore, it can be expected that in the future, the photonics-assisted mmWave and THz architecture can not only effectively improve the performance of communication, but also improve the performance of sensing.

In cases where the processing capability of the network nodes of ISAC is limited, a centralized processing architecture will be useful. The fiber network can effectively connect each node, send the sensing information to the central office for centralized processing, and realize the dynamic sensing of moving vehicles and collaborative sensing through multiple base stations. The central office can also aggregate and jointly process the information from the vehicles of their surrounding environments such as other vehicles or pedestrians to achieve a more powerful network of sensing functions.

W-band photonics-assisted experiments now provide a progression from flexible waveform sharing to sensing-assisted communication. An adaptive-waveform fiber-wireless system demonstrated that photonic generation can allocate waveform resources between sensing and communication[68]. Radar-aided flexible communication then used sensing results to support communication adaptation in a distributed W-band architecture[69], while CE-LFM-OFDM combined a constant-envelope linear-frequency-modulated component with OFDM for flexible integrated operation[70]. These results are compatible with a centralized architecture: coherent optical references and sensing data can be distributed through fiber, processed at the central office, and returned for beam control, blockage recovery, waveform selection, and link adaptation. Practical photonic ISAC must account for leakage

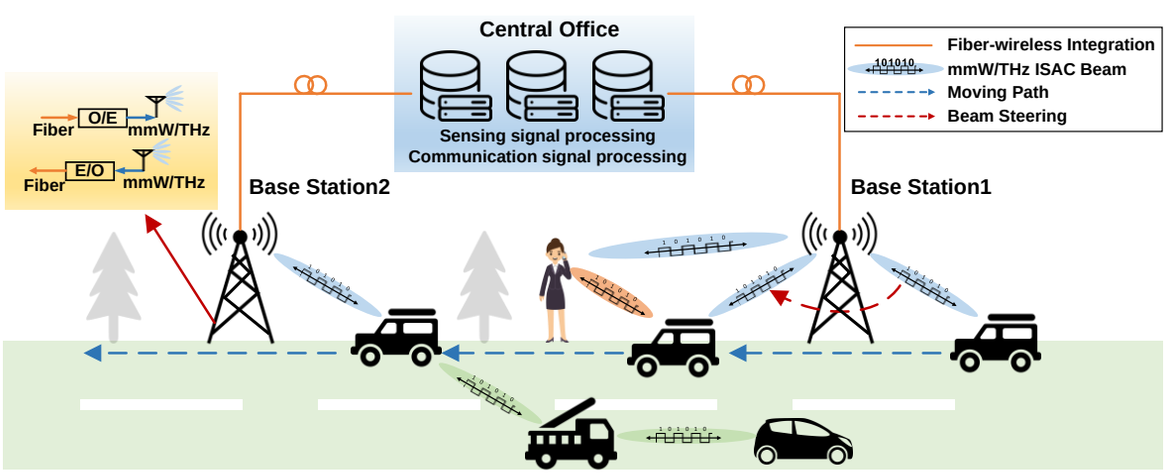

Fig. 12 ISAC scenarios in photonics-assisted mmWave and THz 6G system
图 12 光子辅助毫米波与太赫兹 6G 系统中的通信感知一体化(ISAC)应用场景

and dynamic range when sensing and communication share hardware, and for timing and phase synchronization across fiber-distributed nodes. Evaluation should jointly report communication net rate and error performance, sensing resolution and accuracy, update latency, and the optical/RF power budget. Large bandwidth alone does not establish accurate sensing under mobility, multipath, or synchronization drift[67,71]. Related photonic radar and THz-over-fiber ISAC demonstrations are reported in Refs. [72-74].

4 Conclusions

Photonics-assisted mmWave and THz communication provides broadband signal generation, flexible frequency conversion, and low-loss distribution for future fiber-wireless systems. Integrated sources, MUTC photodiodes, thin-film lithium niobate interfaces, plasmonic and graphene devices, fiber-wireless-fiber links, MIMO transmission, and learning-assisted equalization have expanded the capabilities of photonics-assisted architectures. Photonics is particularly effective for frequency-agile carrier generation, broadband conversion, coherent reference sharing, remote distribution, and true-time-delay beamforming, while electronics remains essential for power amplification, low-noise reception, data conversion, control, and digital signal processing. The immediate priorities are to improve linear RF output and receiver conversion sensitivity at a declared power budget, validate heterogeneous modules across temperature and manufacturing variation, and demonstrate real-time DSP and beam control with measured latency and energy per delivered bit. Longer-term scaling should then be assessed using multi-node fiber-wireless and ISAC experiments under matched rate, reach, and reliability conditions. These requirements call for an optoelectronic architecture in which each function is assigned according to its bandwidth, power, and integration constraints.

Common abbreviation list

6G Sixth-generation wireless communication

ACE Antenna-coupled-electrode

ADC Analog-to-digital converter

AE Autoencoder

AI Artificial intelligence

ASIC Application-specific integrated circuit

AWGN Additive white Gaussian noise

BER Bit error rate

CC-MUTC Charge-compensated modified uni-travelling carrier

CE-LFM-OFDM Constant-envelope linear-frequency-modulated orthogonal frequency-division multiplexing

CMOS Complementary metal – oxide – semiconductor

Co-Rx Coherent receiver

CU Central unit

DAC Digital-to-analog converter

DFB Distributed-feedback laser

DNN Deep neural network

DSP Digital signal processing

DU Distributed unit

E/O Electrical-to-optical

EIC Electronic integrated circuit

Elec. Rx Electronic receiver

eMBB+ Enhanced mobile broadband, evolved scenario

ETOR Electronic transmitter with optical receiver

FDM Frequency-division multiplexing

FEC Forward-error correction

FPGA Field-programmable gate array

FTN Faster-than-Nyquist

GS Geometric shaping

HS Hybrid shaping

IEEE Institute of Electrical and Electronics Engineers

IF Intermediate frequency

ISAC Integrated sensing and communication

ISI Intersymbol interference

ITU International Telecommunication Union

LD Laser diode

LNA Low-noise amplifier

LO Local oscillator

MCF Multicore fiber

MIMO Multiple-input multiple-output

MMF Multimode fiber

MMIC Monolithic microwave integrated circuit

mmWave Millimeter wave

mMTC+ Massive machine-type communications, evolved scenario

Mod. Modulator

MRC Maximal-ratio combining

MUTC Modified uni-travelling carrier

MUTC-PD Modified uni-travelling-carrier photodiode

MZM Mach – Zehnder modulator

NLOS Non-line-of-sight

O/E Optical-to-electrical

OAM Orbital angular momentum

OFDM Orthogonal frequency-division multiplexing

Opt. Tx Optical transmitter

OTER Optical transmitter with electronic receiver

OTFS Orthogonal time-frequency space

OTOR Optical transmitter with optical receiver

PCU Phase control unit

PD Photodiode

PDM Polarization-division multiplexing

PIC Photonic integrated circuit

PIN-PD p – i – n photodiode

PIN/UTC-PD p – i – n/uni-travelling-carrier photodiode

PM Phase modulator

PS Probabilistic shaping

QAM Quadrature amplitude modulation

QCL Quantum cascade laser

QPSK Quadrature phase-shift keying

RAN Radio access network

RAT Radio access technology

RF Radio frequency

RIS Reconfigurable intelligent surface

RoF Radio over fiber

RRU Remote radio unit
Rx Receiver
SCM Single-carrier modulation
SDM Space-division multiplexing
SMF Single-mode fiber
SNR Signal-to-noise ratio
sub-THz Sub-terahertz
TCA Tightly coupled array
TFLN Thin-film lithium niobate
THz Terahertz
TIA Transimpedance amplifier
TTD True time delay
Tx Transmitter
UE User equipment
URLLC+ Ultra-reliable low-latency communications, evolved scenario
UTC Uni-travelling carrier
UTC-PD Uni-travelling-carrier photodiode
V2X Vehicle-to-everything
WDM Wavelength-division multiplexing
xR Extended reality

References

[1] NTT DOCOMO. White paper: 5G evolution and 6G (Version 1.0) [R/OL]. 2020[2026-08-17].
[2] Nagatsuma T, Ducournau G, Renaud C C. Advances in terahertz communications accelerated by photonics [J]. Nature Photonics, 2016, 10: 371-379.
[3] Elayan H, Amin O, Shihada B, et al. Terahertz band: The last piece of RF spectrum puzzle for communication systems [J]. IEEE Open Journal of the Communications Society, 2020, 1: 1-32.
[4] Rappaport T S, Xing Y, Kanhere O, et al. Wireless communications and applications above 100 GHz: Opportunities and challenges for 6G and beyond [J]. IEEE Access, 2019, 7: 78729-78757.
[5] ITU-R. Framework and overall objectives of the future development of IMT for 2030 and beyond: Recommendation ITU-R M. 2160-0[EB/OL]. 2023[2026-08-17].
[6] Waterhouse R, Novack D. Realizing 5G: Microwave photonics for 5G mobile wireless systems [J]. IEEE Microwave Magazine, 2015, 16(8): 84-92.
[7] Nagatsuma T, Ohtake H, Kato K, et al. Photonics-empowered terahertz wireless communications [C]. 2023 24th International Conference on Applied Electromagnetics and Communications (ICECOM). 2023: 1-3.
[8] Jia S, Lo M C, Zhang L, et al. Integrated dual-laser photonic chip for high-purity carrier generation enabling ultrafast terahertz wireless communications [J]. Nature Communications, 2022, 13: 1388.
[9] Montanaro A, Piccinini G, Mišeikis V, et al. Sub-THz wireless transmission based on graphene-integrated optoelectronic mixer [J]. Nature Communications, 2023, 14: 6471.
[10] Tao Z, Wang H, Feng H, et al. Ultrabroadband on-chip photonics for full-spectrum wireless communications [J]. Nature, 2025, 645: 80-87.
[11] Sun S, Wang B, Liu K, et al. Integrated optical frequency division for microwave and mmWave generation [J]. Nature, 2024, 627: 540-545.
[12] Li L, Long T, Yang X, et al. Modified uni-travelling-carrier photodiodes with 206 GHz bandwidth and 0.81 A W^{-1} external responsivity [J]. Nature Photonics, 2025, 19: 1301-1308.
[13] Tian Y, Li Y, Xiong B, et al. D-band MUTC photodiode module for ultra-wideband 160 Gbps photonics-assisted fiber-THz integrated communication system [J]. Laser & Photonics Reviews, 2025, 19: 2401459.
[14] Tian Y, Li Y, Dong B, et al. High-power MUTC photodiode module for photonics-assisted beyond 100 Gb/s wireless sub-THz communications in the F-band [J]. Journal of Lightwave Technology, 2024, 42(16): 5616-5623.
[15] Zhang Y, Yang J, Zeng Y, et al. Monolithic lithium niobate photonic chip for efficient terahertz-optic modulation and terahertz generation [J]. Nature Communications, 2025, 16: 10330.
[16] Guo Y, Zhang X, Zhang Y, et al. Minimalist terahertz wireless transceiver in integrated photonics [J]. Nature Communications, 2026, 17: 4429.
[17] Soundarapandian K P, Castilla S, Koepfli S M, et al. High-speed graphene-based sub-terahertz receivers enabling wireless communications for 6G and beyond [J]. Nature Communications, 2026, 17: 2627.
[18] Blatter T, Koepfli S M, Zuerrer A, et al. All-plasmonic sub-terahertz wireless communication link [J]. Nature Communications, 2025, 16: 9988.
[19] Zhang L, Pang X, Jia S, et al. Beyond 100 Gb/s optoelectronic terahertz communications: Key technologies and directions [J]. IEEE Communications Magazine, 2020, 58(11): 34-40.
[20] Li X, Yu J. Generation and heterodyne detection of >100-Gb/s Q-band PDM-64QAM mm-wave signal [J]. IEEE Photonics Technology Letters, 2017, 29(1): 27-30.
[21] Steeg M, Exner F, Tebart J, et al. 100 Gbit/s V-band transmission enabled by coherent radio-over-fiber system with IF-OFDM envelope detection and SSBI suppression [C]. 2020 XXXIIIrd General Assembly and Scientific Symposium of the International Union of Radio Science (URSI GASS). 2020: 1-4.
[22] Uchida D, Kawaguchi T, Yoda D, et al. A novel E-band testbed for polarization MIMO-OFDM systems with wideband IQ imbalance compensation [C]. 2020 IEEE Wireless Communications and Networking Conference (WCNC). 2020: 1-7.
[23] Dat P T, Rottenberg F, Kanno A, et al. 132 Gb/s 3 × 3 full MIMO fiber-wireless seamless system in W band using WDM/PDM RoF transmission [C]. 2020 European Conference on Optical Communications (ECOC). 2020: 1-4.
[24] Kanno A, Dat P T, Umezawa T, et al. Field trial of 1.5-Gbps 97-GHz train communication system based on linear cell radio over fiber network for 240-km/h high-speed train [C]. Optical Fiber Communication Conference (OFC). 2019: Th4C.2.
[25] Wang K, Zhao L, Yu J. 200 Gbit/s photonics-aided MMW PS-OFDM signals transmission at W-band enabled by hybrid time-frequency domain equalization [J]. Journal of Lightwave Technology, 2021, 39(10): 3137-3144.
[26] Dat P T, Yamaguchi Y, Inagaki K, et al. Transparent fiber-radio-fiber bridge at 101 GHz using optical modulator and direct photonic down-conversion [C]. Optical Fiber Communication Conference (OFC). 2021: F3C.4.
[27] Horst Y, Blatter T, Kulmer L, et al. Transparent optical-THz-optical link transmission over 5/115 m at 240/190 Gbit/s enabled by plasmonics [C]. Optical Fiber Communication Conference (OFC). 2021: F3C.1.
[28] Takano K, Amakawa S, Katayama K, et al. A 105Gb/s 300GHz CMOS transmitter [C]. 2017 IEEE International Solid-State Circuits Conference (ISSCC). 2017: 308 – 309.
[29] Jia S, Zhang L, Wang S, et al. 2 × 300 Gbit/s line rate PS-64QAM-OFDM THz photonic-wireless transmission [J]. Journal of Lightwave Technology, 2020, 38(17): 4715-4721.
[30] Tokizane Y, Kishikawa H, Kikuhara T, et al. Beyond 350 GHz: Single-channel 112 Gbps photonic wireless transmission at 560 GHz using soliton microcombs [J]. Communications Engineer-

ing, 2026, 5: 77.
[31] Salamin Y, Benea-Chelmus I C, Fedoryshyn Y, et al. Compact and ultra-efficient broadband plasmonic terahertz field detector [J]. Nature Communications, 2019, 10: 5550.
[32] Elumalai J, Salih M, Fice M, et al. Free-space optical communications at 4 Gbit/s data rate with a terahertz laser[J]. Communications Physics, 2026, 9: 33.
[33] Li Y, Tian Y, Dong B, et al. Demonstration of 123.72-Gbps D-band fiber-THz-fiber system based on full photonic conversion technology with broadband optoelectronic devices[J]. Chinese Optics Letters, 2025, 23(5): 053901.
[34] Long J, Yu J, Wang C, et al. 510-Gbps 322-GHz photonics-aided terahertz wireless transmission system with MIMO embedded adaptive phase recovery equalizer[J]. IEEE Transactions on Microwave Theory and Techniques, 2025, 73(6): 3597-3607.
[35] Xu S, Zhou W, Zhao X, et al. Long-distance 20.1 km THz wireless transmission using CVMSO NN equalizer by photonics-aided technology[J]. IEEE Transactions on Microwave Theory and Techniques, 2025, 73(10): 8210-8219.
[36] Fortier T M, Kirchner M S, Quinlan F, et al. Generation of ultrastable microwaves via optical frequency division[J]. Nature Photonics, 2011, 5: 425-429.
[37] Marin-Palomo P, Kemal J N, Karpov M, et al. Microresonator-based solitons for massively parallel coherent optical communications[J]. Nature, 2017, 546: 274-279.
[38] Corcoran B, Tan M, Xu X, et al. Ultra-dense optical data transmission over standard fibre with a single chip source[J]. Nature Communications, 2020, 11: 2568.
[39] Sung M, Moon S R, Kim E S, et al. Design considerations of photonic THz communications for 6G networks [J]. IEEE Wireless Communications, 2021, 28(5): 185-191.
[40] Mercante A J, Shi S, Yao P, et al. Thin film lithium niobate electro-optic modulator with terahertz operating bandwidth[J]. Optics Express, 2018, 26(11): 14810-14816.
[41] Ummethala S, Harter T, Koehnle K, et al. THz-to-optical conversion in wireless communications using an ultra-broadband plasmonic modulator[J]. Nature Photonics, 2019, 13: 519-524.
[42] Dittmer J, Tebart J, Matalla P, et al. Comparison of electronic and optoelectronic signal generation for (sub-)THz communications[J]. International Journal of Microwave and Wireless Technologies, 2025, 17(2): 246–256.
[43] Ishibashi T, Ito H. Uni-traveling-carrier photodiodes[J]. Journal of Applied Physics, 2020, 127(3): 031101.
[44] Carey V A, Konkol M R, Shi S, et al. Millimeter wave photonic tightly coupled array [J]. IEEE Transactions on Antennas and Propagation, 2021, 69(8): 4488-4503.
[45] Wang C, Zhang M, Chen X, et al. Integrated lithium niobate electro-optic modulators operating at CMOS-compatible voltages [J]. Nature, 2018, 562: 101-104.
[46] He M, Xu M, Ren Y, et al. High-performance hybrid silicon and lithium niobate Mach-Zehnder modulators for 100 Gbit/s and beyond[J]. Nature Photonics, 2019, 13: 359-364.
[47] Zhou W, Zhao L, Zhang J, et al. 135-GHz D-band 60-Gbps PAM-8 wireless transmission employing a joint DNN equalizer with BP and CMMA [J]. Journal of Lightwave Technology, 2020, 38(14): 3592-3601.
[48] Wang K, Zhou W, Zhao L, et al. Bi-directional OFDM truncated PS-4096QAM signals transmission in a full-duplex MMW-RoF system at E-band[J]. Journal of Lightwave Technology, 2021, 39(11): 3412-3419.
[49] Liu C, Wang C, Zhou W, et al. 81-GHz W-band 60-Gbps 64-QAM wireless transmission based on a dual-GRU equalizer[J]. Optics Express, 2022, 30(2): 2364-2377.
[50] Li X, Yu J, Chang G K. Photonics-assisted technologies for extreme broadband 5G wireless communications [J]. Journal of Lightwave Technology, 2019, 37(12): 2851-2865.
[51] Li Y, Dong B, Luo P, et al. Simplified coherent photonics-aided D-band fiber-THz integrated system with adaptive Kramers-Kronig scheme and probabilistic shaping [J]. Journal of Lightwave Technology, 2025, 43(6): 2568-2579.
[52] Lin J, Xu S, Wang Q, et al. D-band 4.6 km 2 × 2 MIMO photonic-assisted terahertz wireless communication utilizing iterative pruning deep neural network-based nonlinear equalization [J]. Photonics, 2024, 11(11): 1009.
[53] Karanov B, Chagnon M, Thouin F, et al. End-to-end deep learning of optical fiber communications [J]. Journal of Lightwave Technology, 2018, 36(20): 4843-4855.
[54] O'Shea T, Hoydis J. An introduction to deep learning for the physical layer [J]. IEEE Transactions on Cognitive Communications and Networking, 2017, 3(4): 563-575.
[55] Zhang H, Zhang L, Wang S, et al. Tbit/s multi-dimensional multiplexing THz-over-fiber for 6G wireless communication [J]. Journal of Lightwave Technology, 2021, 39(18): 5783-5790.
[56] Saitoh K. Multi-core fiber technology for SDM: Coupling mechanisms and design[J]. Journal of Lightwave Technology, 2022, 40(5): 1527-1543.
[57] Chen R, Long W X, Wang X, et al. Multi-mode OAM radio waves: Generation, angle-of-arrival estimation and reception with UCAs[J]. IEEE Transactions on Wireless Communications, 2020, 19(10): 6932-6947.
[58] Lee J, Lee C, Kim J, Seo M. A 140 GHz two-channel transmitter in 40 nm bulk CMOS[J]. Electronics, 2026, 15(11): 2349.
[59] Jia J, Chen J, Dong B, et al. Intelligent end-to-end nonlinear constellation auto-optimization in W-band fiber-MMW integrated transmission for 6G access[C]. Optical Fiber Communication Conference (OFC). 2022: W3I.1.
[60] Wang L, Feng H, Bai L, et al. Heterogeneously integrated photonic terahertz transmitter on thin-film lithium niobate[J]. Nature Communications, 2026, 17: 9797.
[61] Cao Z, Ma Q, Smolders A B, et al. Advanced integration techniques on broadband millimeter-wave beam steering for 5G wireless networks and beyond[J]. IEEE Journal of Quantum Electronics, 2016, 52(1): 1-20.
[62] Di Renzo M, Debbah M, Phan-Huy D T, et al. Smart radio environments empowered by reconfigurable AI meta-surfaces: An idea whose time has come [J]. EURASIP Journal on Wireless Communications and Networking, 2019: 129.
[63] Paul B, Sertel K, Nahar N K. Photonic beamforming for 5G and beyond: A review of true time delay devices enabling ultra-wideband beamforming for mmWave communications [J]. IEEE Access, 2022, 10: 75513-75526.
[64] Meijerink A, Roeloffzen C G H, Meijerink R, et al. Novel ring resonator-based integrated photonic beamformer for broadband phased array receive antennas—Part I: Design and performance analysis [J]. Journal of Lightwave Technology, 2010, 28(1): 3-18.
[65] Zhuang L, Roeloffzen C G H, Hoekman M, et al. Programmable photonic signal processor chip for radiofrequency applications [J]. Optica, 2015, 2(10): 854-859.
[66] Zhang Q, Yu J, Zhao X, et al. 4.6-km D-band photonic-assisted terahertz wireless communication employing SIMO and MRC technology[J]. IEEE Transactions on Microwave Theory and Techniques, 2024, 72(11): 6657-6668.
[67] Pan S, Zhang Y. Microwave photonic radars[J]. Journal of Lightwave Technology, 2020, 38(19): 5450-5484.
[68] Dong B, Jia J, Li G, et al. Demonstration of photonics-based flexible integration of sensing and communication with adaptive waveforms for a W-band fiber-wireless integrated network [J]. Optics Express, 2022, 30(22): 40936-40950.
[69] Jia J, Dong B, Tao L, et al. Demonstration of radar-aided flexible

communication in a photonics-based W-band distributed integrated sensing and communication system for 6G[J]. Chinese Optics Letters, 2024, 22(4): 043901.
[70] Wu F, Dong B, Du P, et al. Photonic-assisted W-band flexible integrated sensing and communication system for fiber-wireless network based on CE-LFM-OFDM[J]. Optics Letters, 2024, 49(16): 4605-4608.
[71] Wang L, Wang X, Pan S. Microwave photonics empowered integrated sensing and communication for 6G[J]. IEEE Transactions on Microwave Theory and Techniques, 2025, 73(8): 5295-5315.
[72] Ghelfi P, Laghezza F, Scotti F, et al. A fully photonics-based coherent radar system[J]. Nature, 2014, 507: 341-345.
[73] Lyu Z, Zhang L, Zhang H, et al. Radar-centric photonic terahertz integrated sensing and communication system based on LFM-PSK waveform[J]. IEEE Transactions on Microwave Theory and Techniques, 2023, 71(11): 5019-5027.
[74] Li L, Zhang L, Zhang H, et al. THz-over-fiber system with orthogonal chirp division multiplexing for integrated sensing and communication[J]. Journal of Lightwave Technology, 2024, 42(1): 176-183.

面向6G的光子辅助毫米波与太赫兹通信:进展、挑战与展望

贾俊连, 董博宇, 迟 楠, 张俊文*
(复旦大学 未来信息创新学院 电磁波信息科学教育部重点实验室,上海 200433)

摘要:光子辅助毫米波与太赫兹通信可为第六代移动通信(6G)提供宽带无线接口,并与光纤网络衔接。本文综述其系统架构、光电转换器件和代表性传输实验,比较波形与数字信号处理、多维复用、波束赋形及通感一体化方案的适用条件。光子技术有利于宽带载波生成、频率调谐、低损耗光纤分发和相干参考共享,但输出功率与转换效率仍限制链路性能,实时处理和封装集成也影响系统能耗及实现成本。因此,架构选择需要同时考虑链路预算、系统能耗和应用需求;异质集成及器件、电路与天线的联合设计是后续研究的重点。

关 键 词:第六代移动通信;光子辅助通信;毫米波通信;太赫兹通信;光纤无线融合
中图分类号:TN929.5;TN913.7 **文献标识码**:A